Available online at www.sciencedirect.com
SCIENCE DIRECT®
Journal of Nuclear Materials 321 (2003) 238–248
journal of nuclear materials
www.elsevier.com/locate/jnucmat

Effect of Mo addition on the corrosion resistance of Zr-based alloy in water containing LiOH

J.H. Lee, S.K. Hwang *,[1]

School of Materials Science and Engineering, Inha University, Incheon 402-751, Republic of Korea

Received 6 October 2002; accepted 6 May 2003

Abstract

As a sequel to the previous works on the mechanical properties and texture, the corrosion resistance of Mo-containing Zr-base alloys in LiOH-added water was studied. Experimental alloys of Zr–1Nb–1Sn–0.1Fe and Zr–1Nb–1Sn–0.1Fe–xMo ($x = 0$, 0.2, 0.5 wt%), prepared by plasma arc remelting, showed lower weight gains than those of the commercial alloys including Zircaloy-4 and ZIRLO. Mo-addition resulted in a higher corrosion rate in the experimental alloys. Increased corrosion rate in these alloys was associated with lumpy microstructure of oxides with a higher portion of the monoclinic phase. The microstructural characteristic of oxides was attributed to the uneven distribution of β-Zr that was stabilized by Mo. Incomplete recrystallization and decreased normal basal texture also adversely affected the corrosion resistance of the Mo-containing alloys. It was shown, however, that the corrosion resistance of Mo-containing alloys could be improved to the level of the Mo-free alloy by a proper heat treatment to remove the undesirable microstructural feature.

PACS: 28.41.T; 81.65.M; 42.81.B

1. Introduction

Due to advanced design requirement such as high burnup, there are ever-increasing demands on the performance of Zr-base alloys for the nuclear reactor core applications. Accordingly, alloys with improved corrosion resistance have been newly introduced, examples being ZIRLO and E635 [1,2]. These alloys consist of balanced Nb and Sn, approximately 1 wt% each, and a small addition of Fe, typically 0.1 wt%. To enhance the yield strength of this alloy further, Mo-modification of the chemical compositions was studied. It was found that addition of approximately 0.3–0.5 wt% Mo increased the yield strength by about 20% [3–5]. The Mo-addition also resulted in microstructural refinement, suppression of abnormal grain growth and enhanced damage tolerance under electron irradiation [6,7]. However, the water corrosion resistance of the Mo-modified alloy has not been evaluated so far.

The purpose of the present work was to assess the corrosion resistance of experimental Zr–1Nb–1Sn–0.1Fe–xMo alloy in water containing LiOH. Particular point of interest was the effect of heat treatment condition on the microstructure such as the extent of recrystallization and second phase particle distribution in the experimental alloys and their consequences on the corrosion resistance.

2. Experimental procedure

Chemical composition of the experimental alloys was designed on the basis of Zr–1Nb–1Sn–0.1Fe with 0, 0.2 and 0.5 wt% Mo, respectively. Sponge-type Zr (99.5%)

* Corresponding author. Tel.: +82-32 860 7537; fax: +82-32 862 5546.
E-mail address: skhwang2@inha.ac.kr (S.K. Hwang).
[1] Jointly appointed at the Center for the Advanced Aerospace Materials, Pohang, 790-784, Korea.

0022-3115/$ - see front matter © 2003 Elsevier B.V. All rights reserved.
doi:10.1016/S0022-3115(03)00275-7

Table 1
Chemical compositions of experimental alloys

Nominal	Analysis [wt%]				
	Nb	Sn	Mo	Fe	Zr[a]
Zr–1Nb–1Sn–0.1Fe	0.97	1.03	–	0.16	Balance
Zr–1Nb–1Sn–0.2Mo–0.1Fe	1.01	1.06	0.22	0.13	
Zr–1Nb–1Sn–0.5Mo–0.1Fe	0.95	1.07	0.50	0.13	

[a] The nuclear grade sponge Zr used in the present study contained 38 ppm carbon, 530 ppm oxygen, 422 ppm Fe, 44 ppm Hf and 10 ppm Si prior to melting. During melting and subsequent treatments, the residual oxygen content of these alloys increased to approximately 1000 ppm.

produced by Teledyne Wah Chang and Nb (99.9%), Mo (99.95%), Sn (99.95%) and Fe (99.95%) purchased from CERAC Co. were used for making experimental alloys. Alloys were prepared by plasma arc remelting into buttons of approximately 300 g each. The result of the chemical analysis is shown in Table 1. Subsequent processing of the experimental alloys consisted of forging (1100 °C, 50%), homogenization (1000 °C/20 min), hot rolling (800 °C, 50%), β-annealing (1000 °C/10 min, furnace cooling), cold rolling (75%) and recrystallization annealing. Four annealing heat treatment conditions were employed: 570 °C/16 h, 600 °C/8 h, 600 °C/16 h and 650 °C/32 h followed by furnace cooling.

Corrosion test was conducted according to ASTM G2-88 in water containing 220 ppm LiOH at 360 °C pressurized at 17.9 MPa. Up to 100 days of exposure was made in autoclaves. Specimens for optical microscopy were obtained by an etchant consisting of H_2O, HNO_3 and HF in the ratio of 50:45:5 in volume. Specimens for transmission electron microscopy (TEM) were prepared by a jet polisher containing electrolyte solution containing of $HClO_4$ and CH_3OH in the ratio of 10:90 in volume maintained at −45 °C. For the analysis of second phase particles, TEM micrographs were used: using 10 micrographs of various magnifications, the number density and the mean size of the distribution were obtained. For oxide phase analysis, X-ray diffraction (XRD) method was employed, using Cu-K_α under acceleration condition of 40 kV and 40 mA and with the operating parameters of 0.5° s^{-1} scan rate and the incident angle of 5° in the range of 25–40° [$2\theta_0$]. The thickness of oxides ranged typically from 2 to 6 μm. Kearns number, f_n, was obtained from the inverse pole figure by calculating the average (0 0 0 1) pole intensity normal to the sample surface. The stress state in the oxide layer was studied by a Micro-area X-ray diffractometer (Rigaku DMAX PSPC MDG2000).

3. Results

3.1. Corrosion resistance of experimental alloys

Compared to commercial Zr-base alloys and other experimental alloys, the present experimental alloys showed a good corrosion resistance when they were heat-treated properly. This is illustrated in Fig. 1 that compares the published data of conventional Zircaloy-4, improved Zircaloy-4, β-quenched Zircaloy-4, ZIRLO [8], an experimental alloy reported by Kim et al. [9] with the present experimental alloy Zr–1Nb–1Sn–0.1Fe–0.5Mo heat treated at 600 °C/16 h. The two experimental alloys, the modified Zircaloy-4 by Kim et al. [9] and the present alloy with Mo modification, showed better corrosion resistance than the commercial alloys. There was a rather large discrepancy between the published data of ZIRLO [8,10] shown in Fig. 1 and that of the present experimental ZIRLO alloy, Zr–1Nb–1Sn–0.1Fe, shown in Fig. 2, which is attributed to the impurity level and the processing details between the commercial alloy and the laboratory alloy.

Within the current experimental alloy compositions, the effect of Mo addition on the corrosion resistance sensitively varied with the heat treatment conditions. As shown in Fig. 2, the corrosion rate increased with Mo content under most heat treatment conditions. The deteriorating trend was severe for the heat treatments of 570 °C/16 h and 650 °C/32 h. However, it is noted in Fig. 2 that the corrosion resistance of the Mo-containing

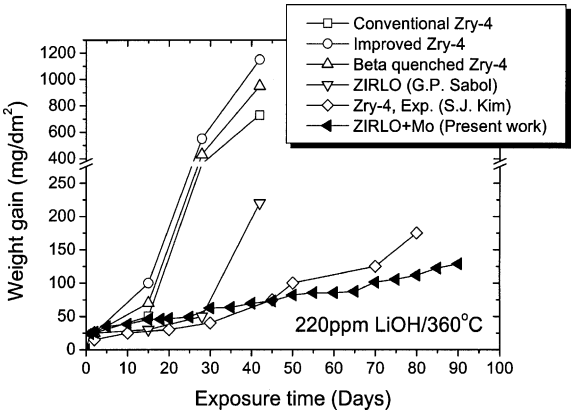

Fig. 1. Weight gains of various Zr-base alloys in water containing LiOH. Comparison of data was made from the Refs. [8,9].

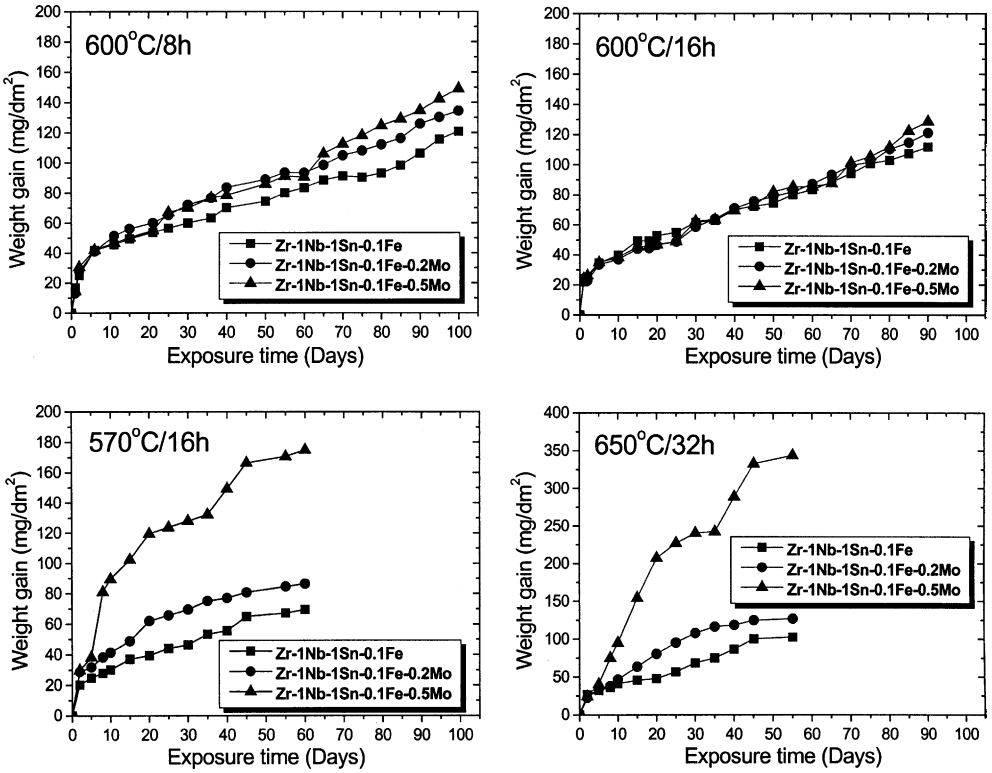

Fig. 2. Weight gains in water containing LiOH of present experimental alloys heat-treated under various conditions. Note that Mo addition is relatively harmless under the annealing heat treatment at 600 °C/16 h whereas it is detrimental under insufficient (570 °C) or excessive (650 °C) annealing conditions.

Table 2
The '*n*' value in pre-transition for corrosion kinetics of Zr–1Nb–1Sn–0.1Fe (ZIRLO) + *x*Mo alloys in 220 ppm LiOH condition

Composition	Heat treatment condition			
	570 °C/16 h	600 °C/8 h	600 °C/16 h	650 °C/32 h
Zr–1Nb–1Sn–0.1Fe	0.386	0.383	0.366	0.430
Zr–1Nb–1Sn–0.2Mo–0.1Fe	0.373	0.438	0.388	0.589
Zr–1Nb–1Sn–0.5Mo–0.1Fe	0.526	0.445	0.377	0.853

Corrosion kinetics, $\Delta w = kt^n$, where Δw, weight gain (mg/dm^2); t, exposure time (days) and k, constant. The 'n' values were acquired from the data used for Fig. 1.

alloys can be made comparable to that of Mo-free Zr–1Nb–1Sn–0.1Fe. With the heat treatment at 600 °C/16 h, the corrosion resistance of the alloys was unaffected by Mo addition over most of the test period.

Except for the most deleterious heat treatment conditions, the corrosion rates of the experimental alloys were rather low and did not show abrupt transition into an accelerated rate. For the case of 570 °C annealing and 650 °C annealing, the corrosion rate significantly increased with Mo content, particularly in the early stage. The absence of the abrupt transition in the corrosion rate of the experimental alloys heat treated at 600 °C/16 h was confirmed by the measurement of the corrosion rate constant as defined by the following equation:

$$\Delta w = kt^n, \tag{1}$$

where Δw is the weight gain, k is a constant and t is exposure time. From Fig. 2, the corrosion rate constant n was calculated and the result is shown in Table 2. The values of n for most experimental alloys heat treated at 600 °C were in the range of 0.37–0.59, which correspond to the pre-transition region [11]. For the alloys heat-treated at 650 °C/32 h, an n value of approximately

0.85 was obtained, which is close to the value corresponding to the post-transition region.

3.2. Microstructure and texture of experimental alloys

In β-annealed condition, lath structures were formed as shown in Fig. 3, regardless of the Mo content. This is due to the β to α transformation. Within the same microstructure, however, Mo-addition resulted in a refinement of the lath dimensions as evidenced by comparing Fig. 3(a) with (b). The average thickness and the length of the α laths were reduced by approximately a factor of two by Mo-addition. This result is consistent with the result previously reported by Chun et al. [3]. During growth of the alpha laths from the β phase upon cooling, Mo atoms appear to retard the solute diffusion rate at the advancing front of α plates as well as that at the interlamellar interface since they partition in the β phase.

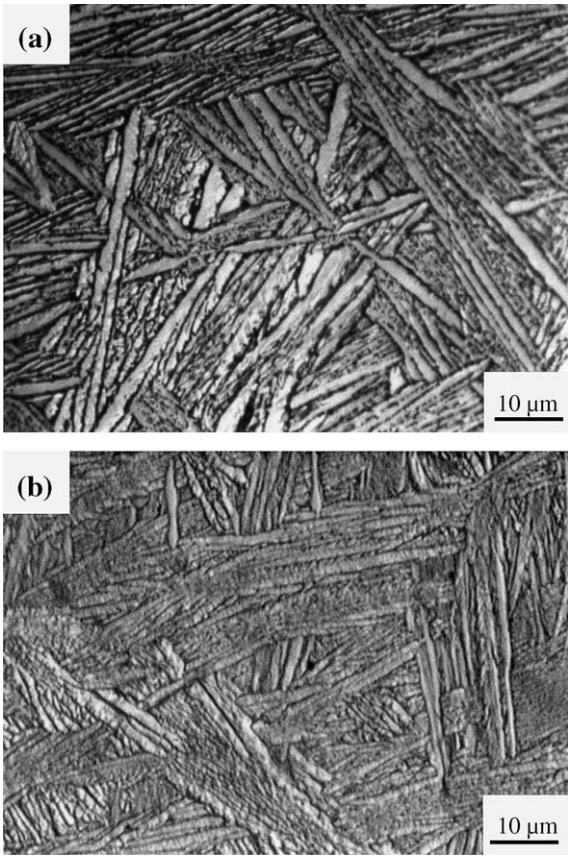

Fig. 3. Optical micrographs of (a) Zr–1Nb–1Sn–0.1Fe and (b) Zr–1Nb–1Sn–0.5Mo–0.1Fe alloy, all beta annealed at 1000 °C for 10 min and furnace cooled. Note the α-lath-refining effect of Mo.

Another significant effect of Mo was retardation of the recrystallization. In Fig. 4, two sets of micrographs are presented, one for Mo-free and another for Mo-containing compositions for two different heat treatment conditions, 600 °C/8 h and 600 °C/16 h. From the comparison of the micrographs, it is clear the 600 °C/8 h heat treatment resulted in complete recrystallization in the Mo-free composition but not in the Mo-containing composition. In the latter case, therefore, some regions of incomplete recrystallization were identifiable – see Fig. 4(b). The extended heat treatment of 16 h at 600 °C, on the other hand, resulted in full recrystallization in both compositions. Therefore the microstructure of heat-treated samples consisted of equiaxed grains. In this case, also, the effect of Mo as a kinetics-retardant was apparent in that the size of recrystallized grains was considerably smaller in the Mo-containing composition: the average size of equiaxed alpha grains was reduced from 2.2 ± 0.6 μm to 1.4 ± 0.3 μm by addition of 0.5 wt% Mo as shown in Fig. 4(c) and (d).

In the Mo-containing specimens the second phase particles showed a heterogeneous distribution, shown as the aligned second phase particles in Fig. 5. Although the aligned feature of second phase particles was locally visible in all present experimental alloys the trend was more pronounced in the Mo-containing composition and in the specimens insufficiently annealed. The pattern of precipitates alignment was consistent with the site of interlamellar β-Zr, which indicates that the β phase became the precursor for the second phase particles. This is considered to be another consequence of the β-stabilizing effect of Mo.

Under all recrystallization heat treatment conditions, Mo-addition increased the number density of second phase particles. As shown in Fig. 6, this effect was most notable in specimens partially recrystallized at 600 °C. The increased amount of second phase particles with Mo content is related to the interlamellar precipitation since the interlamellar spacing decreased with Mo content. During extended annealing at higher temperature, especially at 650 °C for 32 h as shown in Fig. 6(b), particles coarsening occurred regardless of Mo content. In this process, Mo has a mild effect on the rate of particle coarsening and a large effect on the number density of particles.

In agreement with earlier report [3], Mo-addition, especially in the heat treatment conditions, 600 °C/8 h and 650 °C/32 h, was found to decrease the basal pole intensity normal to the surface of plate as shown in Fig. 7. Reduction of the texture intensity originated from the suppression of twinning activity in small-grained materials [12], which is applicable to the present Mo-containing alloys. The Mo effect on texture was particularly pronounced in fully recrystallized (650 °C/32h) sample. Therefore the fraction of (0 0 0 1) surface exposed to the surface of corrosion test sample decreased with Mo

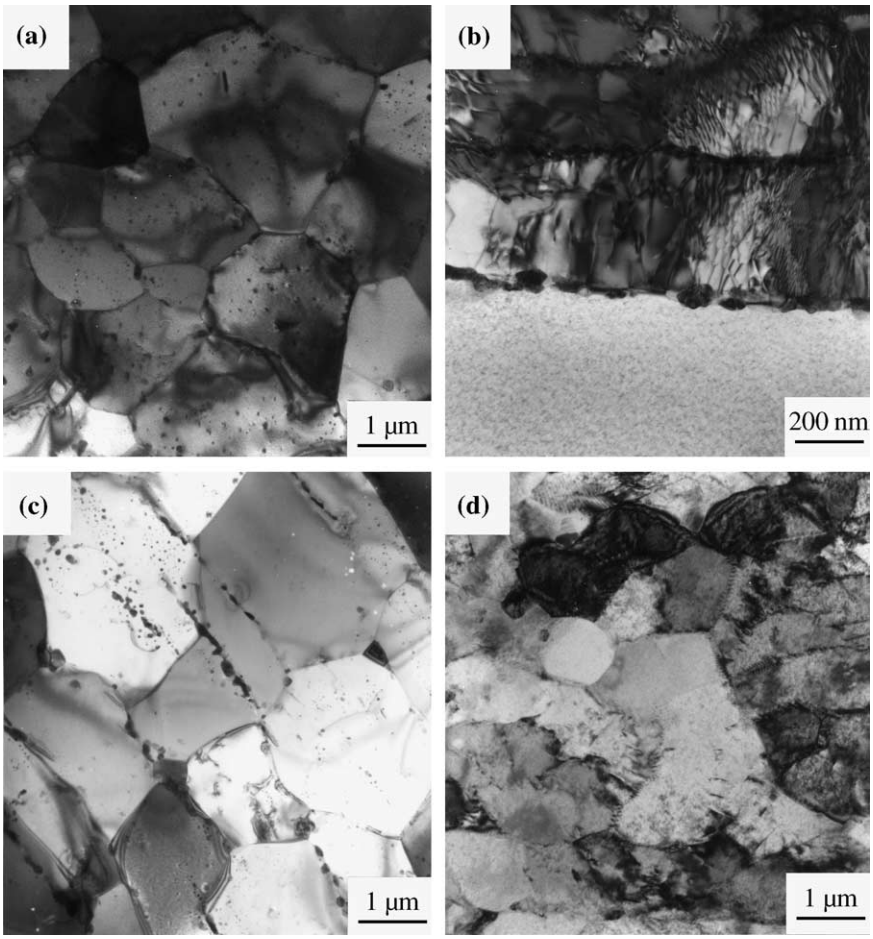

Fig. 4. TEM micrographs of (a) Zr–1Nb–1Sn–0.1Fe annealed at 600 °C/8 h, (b) Zr–1Nb–1Sn–0.1Fe–0.5Mo alloy, 600 °C/8 h, (c) Zr–1Nb–1Sn–0.1Fe annealed at 600 °C/16 h and (d) Zr–1Nb–1Sn–0.1Fe–0.5Mo annealed at 600 °C/16 h, showing the effect of Mo in retarding recrystallization and grain coarsening. Recrystallization is complete in (a) but incomplete in (b) whereas it is complete in (c) and (d). The grain size of recrystallized Mo-containing alloy in (d) is considerably smaller than that of the Mo-free alloy in (c).

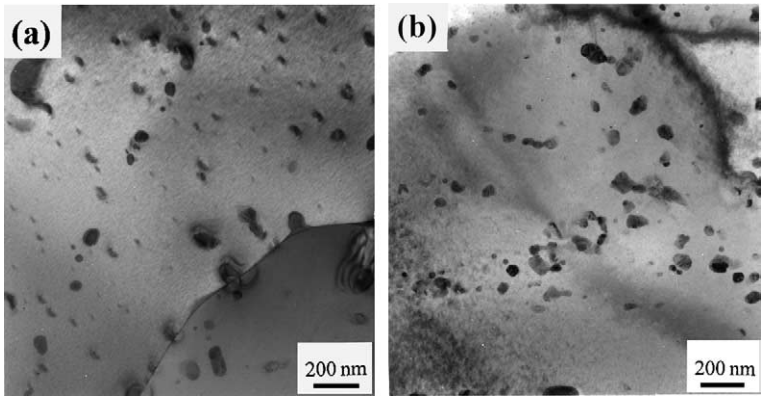

Fig. 5. TEM micrographs of second phase particles in (a) Zr–1Nb–1Sn–0.1Fe and (b) Zr-1Nb–1Sn–0.5Mo–0.1Fe alloy, all heat-treated at 600 °C/8 h, showing the Mo-effect of aligning the particles.

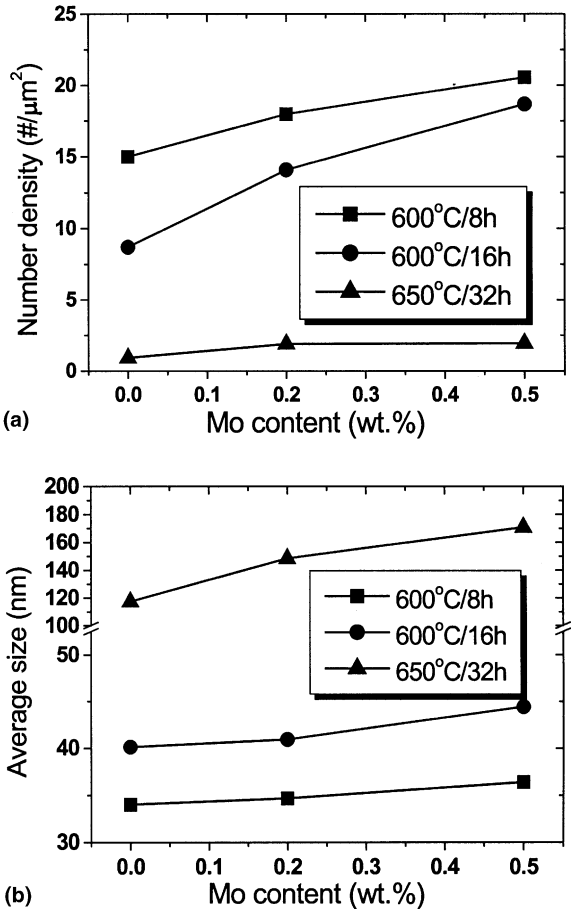

Fig. 6. Effect of Mo-addition on (a) the number density and (b) the mean size of second phase particles in experimental alloys. Note that Mo significantly increased the number density of second phase particles and a slight coarsening effect for the heat treatment at 600 °C/16 h.

content, although it still exceeded the value for the random texture, 0.33. In partially recrystallized state (600 °C), however, the effect of Mo on texture was minimal. Being a plane of low surface energy [13], the basal plane of Zr is known to have the relatively high resistance to corrosion [14]. Within the same chemical composition, therefore, a weakened normal basal texture means a lowered corrosion resistance.

3.3. Microstructural characteristics and stress state of oxides

As shown in Fig. 1, the difference in the corrosion resistance of various alloys appeared early in the test. Therefore, tests were interrupted at an early stage and the microstructural characteristics of oxides in each alloy at this stage were examined. From this study, some

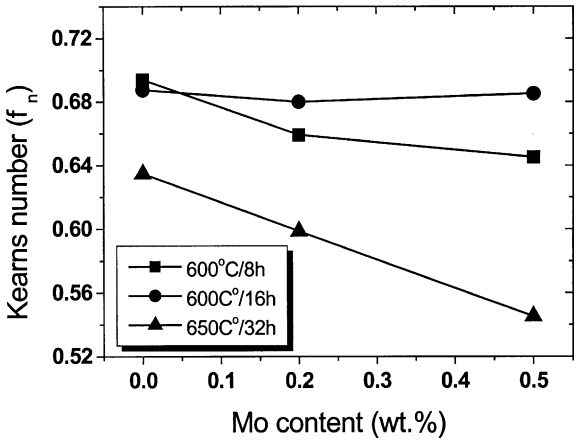

Fig. 7. Variation of the normal basal texture of the experimental alloys annealed at various conditions as a function of Mo content.

differences in the microstructural characteristics of oxides were recognized.

Mo-addition affected the oxide morphology in the early stage of corrosion. This is shown in Fig. 8, which compares the microstructure of oxides in two alloys, Zr–1Nb–1Sn–0.1Fe alloy and Zr–1Nb–1Sn–0.1Fe–0.5Mo alloy, both heat treated identically at 600 °C/8 h and corrosion tested up to the time corresponding to a weight gain of 25 mg/dm^2. The Mo-free alloy showed mostly fine granular oxides. In the Mo-containing alloy, however, the fine granular oxides coexisted with lumpy oxides, the latter being the major constituent. The lumpy oxides have been reported as a consequence of a preferential acceleration of corrosion along the sensitive path such as grain boundaries and particularly oriented lattice planes of weak corrosion resistance.

Oxides in Zr-base alloys are mixtures of two phases, tetragonal phase and monoclinic phase, the ratio of which varies with the chemical composition of alloy and heat treatment. The volume fraction of tetragonal oxides was analyzed at three different stages of corrosion, 25, 50 and 100 mg/dm^2, and for three different levels of Mo content in the present experimental alloys. For the measurement of the volume fraction of tetragonal oxides, V_{ft}, the following equation of Gravie–Nicholson [15] was used:

$$V_{ft} = \frac{I_{t(1\,1\,1)}}{I_{t(1\,1\,1)} + I_{m(1\,1\,1)} + I_{m(\bar{1}\,1\,1)}}, \tag{2}$$

where $I_{j(h\,k\,l)}$ is the XRD peak intensity from $(h\,k\,l)$ plane of jth phase, and the subscripts t and m refer to tetragonal oxide and monoclinic oxide, respectively. Application of the above equation is not warranted in the sense of the absolute amount of a particular oxide phase in a multi-phase matrix especially when the phase of

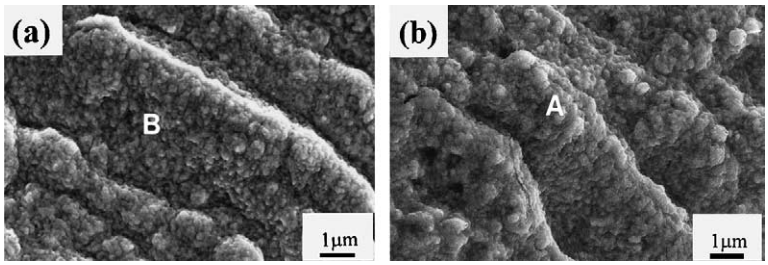

Fig. 8. Oxide morphology on the surface (near the oxide/metal interface) of Zr alloys formed during corrosion test of up to a weight gain of 25 mg/dm^2: (a) Zr–1Nb–1Sn–0.1Fe alloy and (b) Zr–1Nb–1Sn–0.1Fe–0.5Mo alloy. Samples were identically heat treated at 600 °C/8 h. Note the fine-scale microstructural difference; mostly fine-grained feature in the Mo-free alloy vs. lumpy feature in the Mo-containing alloy.

interest is textured. However a relative variation of the phase content can be traced down using Eq. (2) provided that the production sequence of experimental material and the method of XRD specimen preparation are consistent, which was done in the present work.

As shown in Fig. 9, the volume fraction of tetragonal oxides decreased with the weight gain as well as with the Mo content in the alloys regardless of the annealing heat treatment condition. There was also an effect of alloy chemical composition on the morphology of the oxide layer. Two different forms of oxides are shown in Fig. 10, one from Zr–1Nb–1Sn–0.1Fe (Fig. 10(a)) and another from Zr–1Nb–1Sn–0.1Fe–0.5Mo (Fig. 10(b)), which were heat treated identically at 600 °C/8 h and corrosion tested up the a weight gain of 50 mg/dm^2. The specimen containing Mo showed a higher volume fraction of the lumpy oxide whereas the Mo-free specimen showed more needlelike feature. With the progress of corrosion, the oxide morphology is known to change from the needlelike to lumpy feature, which concur with the phase change from tetragonal to monoclinic [16]. Therefore the oxide morphology is consistent with the severer corrosion attack in the Mo-containing alloy.

Quantitative measurement of the stress state in the oxide layer was performed by the method suggested by Wikmark et al. [16]. In this method, the internal stress, σ, of oxide is expressed as

$$\sigma = -\frac{E}{2(1+\nu)} \cot\theta_0 \frac{\pi}{180} \frac{\partial(2\theta)}{\partial(\sin^2\psi)}, \tag{3}$$

where E is Young's modulus, ν is Poisson's ratio, θ_0 is the diffraction angle for the reference plane, ($2\theta_0 = 68.71°$ for (1 3 2) plane), 2θ is the deviation of the diffraction angle and ψ is the incident angle of the X-ray beam.

Prolonged corrosion reduced the compressive stress in the oxide layer of the present experimental alloys and even introduced a tensile stress in some samples. As shown in Fig. 11 this trend was quite general, regardless of the heat treatment time at 600 °C, although the stress conversion from compressive to tensile was more rapid in the partially recrystallized sample (600 °C/8 h). The magnitude of the compressive stress also decreased with the Mo content in the alloys. This result is consistent with the trend of tetragonal oxides described above.

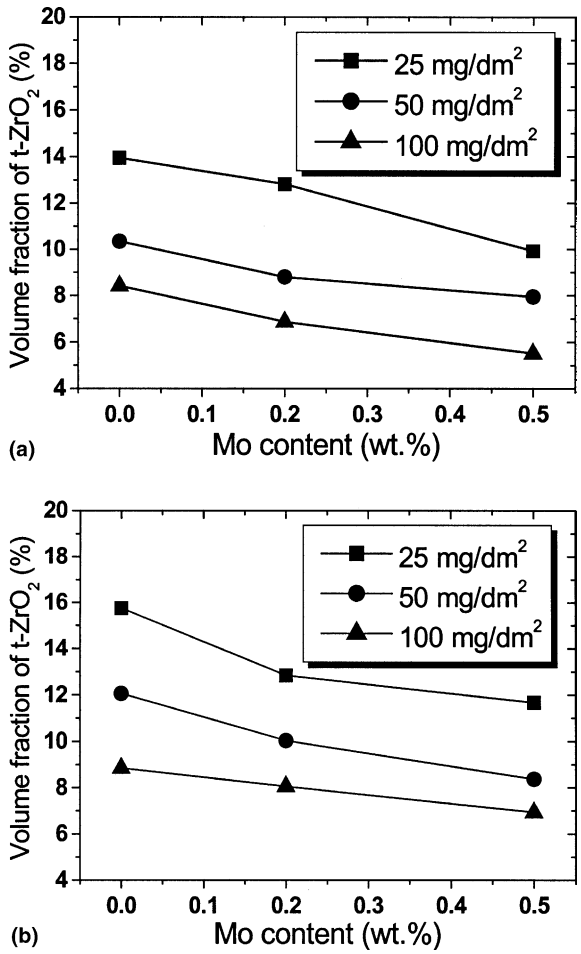

Fig. 9. Effect of Mo content and the weight gain during corrosion test on the amount of tetragonal oxides in the experimental alloys annealed at (a) 600 °C/8 h and (b) 600 °C/16 h.

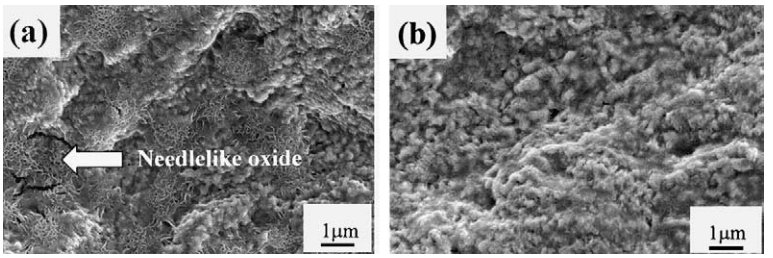

Fig. 10. Oxide morphology on the surface (near the oxide/metal interface) of Zr alloys formed during corrosion test of up to a weight gain of 50 mg/dm^2: (a) Zr–1Nb–1Sn–0.1Fe alloy and (b) Zr–1Nb–1Sn–0.1Fe–0.5Mo alloy. Samples were identically heat treated at 600 °C/8 h. Note the fine-scale microstructural difference; needle-like feature in the Mo-free alloy vs. lumpy feature in the Mo-containing alloy.

The oxides formed during corrosion test showed differences in topological characteristics depending on the alloy composition. Cross-sectional views of the metal/oxide interfaces formed at a weight gain of 50 mg/dm^2 of two alloys, one with Mo and another without Mo, are shown in Fig. 12. In the Mo-free alloy, the metal/oxide interface was smooth whereas the Mo-containing alloy showed numerous irregular protrusions at the interface of metal and oxide. The irregular topological feature at the metal/oxide interface is relevant to the 'lumpy' feature at the external surface of the oxide (Fig. 8).

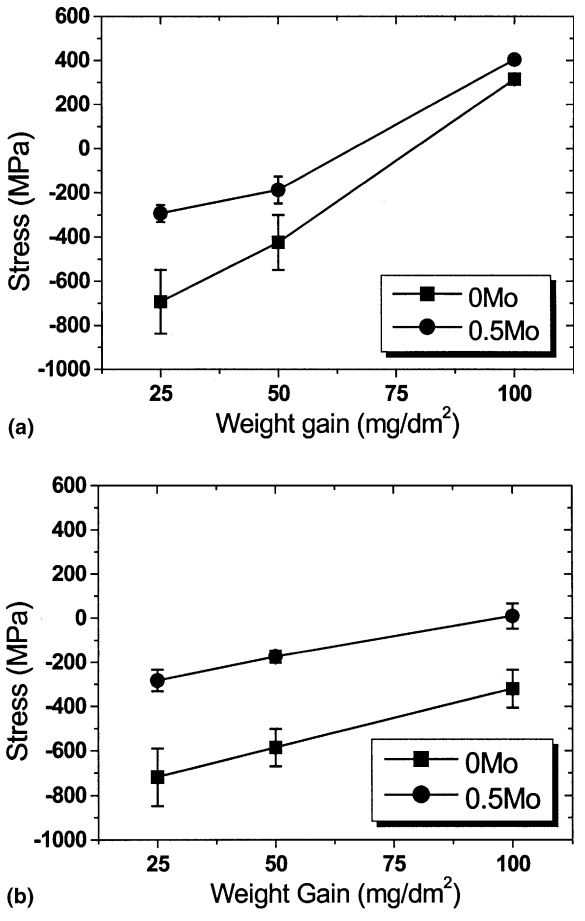

Fig. 11. Variation of the stress state in the oxide layer formed during corrosion test as a function of the weight gain and Mo content in the alloys annealed at (a) 600 °C/8 h and (b) 600 °C/16 h.

4. Discussion

The corrosion characteristics of the present experimental alloys are sensitively related to the microstructure and texture. In terms of the microstructure, the results of Figs. 2, 4 and 6 can be interpreted as signifying that the complete recrystallization with adequate size distribution of second phase particles is essential in improving the corrosion resistance. It is shown in Fig. 4 that insufficient annealing heat treatment produced the microstructure with a high density of dislocations. Particularly, in Mo-containing alloys, the recrystallization rate is low and a heat treatment at 600 °C/8 h did not produce completely recrystallized microstructure of equiaxed grains whereas 600 °C/16 h provided full recrystallization. The improved corrosion resistance by this heat treatment is evidenced in Fig. 2, which also asserts that excessive heat treatment, such as 32 h at 650 °C adversely affects the corrosion resistance. This trend is mainly attributed to the lumpy oxides and in part to coarsening of second phase particles. The reverse transformation temperature determined by DTA was in the range of 650–660 °C upon continuous heating. An XRD analysis revealed about 3–5 vol.% of β-Zr phase in the samples held for 32 h at 650 °C. According to Urbanic and Gilbert [17], filament-type or network type β-Zr is detrimental to corrosion resistance since they result in oxide ridges. Therefore, in order to enhance the corrosion resistance in the Mo-containing alloy, it is crucial to produce the microstructure with two distinct features, complete recrystallization with minimal density of linear defects and suppression of second phase coarsening.

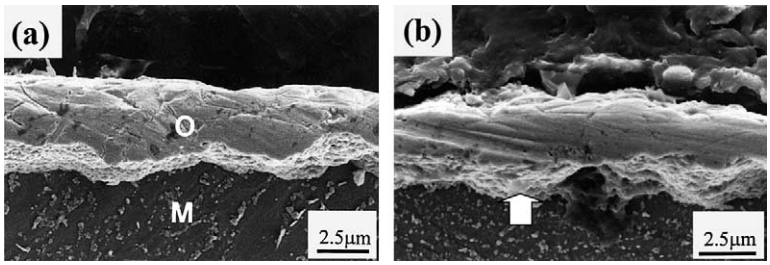

Fig. 12. Cross-sectional SEM micrographs of ZrO_2 formed at a weight gain of 50 mg/dm^2: (a) Zr–1Nb–1Sn–0.1Fe and (b) Zr–1Nb–1Sn–0.1Fe–0.5Mo, both heat-treated at 600 °C/8 h. The samples were tilted so that the bottom surface of the interface is partly in view. Note that the interface of oxide (O) and the metal matrix (M) is smooth for the sample (a) but that of sample (b) has irregular protrusions (see the arrow mark).

The microstructural features described above are also the desirable attributes of cladding material for high burnup fuels. The harsh conditions of the high burnup raise the issue of microstructural stability as a major concern in cladding material. Linear defects such as dislocations tend to increase the susceptibility of cladding for irradiation growth and creep while coarsening of second phase particles may weaken the corrosion resistance. This is because a high dislocation density remaining in the cladding material provides accelerated diffusion, albeit heterogeneous, which results in undesirable microstructural evolution. Molybdenum in solid solution, on the contrary, counter-balances the kinetics of microstructural coarsening through diminishing the diffusivity.

As for the improved corrosion resistance of the Mo-containing alloy heat treated at 600 °C/16 h, the microstructural distribution of second phase particles is relevant. During this heat treatment, second phase particles became more uniformly distributed, the feature known to be beneficial for the corrosion resistance [17]. The reason for the increased uniformity in particle distribution is twofold: growth of pre-existing particles and generation of new particles. Nucleation of additional particles is possible because of supersaturated Mo in the matrix. Due to the low diffusivity of Mo, precipitation is incomplete within 8 h at 600 °C. Newly precipitated particles with a hcp crystal structure as shown in Fig. 13, contain high level of Mo in addition to Nb, which was confirmed by a STEM analysis.

Phase transition in oxide is also relevant to the corrosion rate. It is known that compressive stress promotes formation of tetragonal ZrO_2 rather than monoclinic ZrO_2 [18,19]. During cooling to room tem-

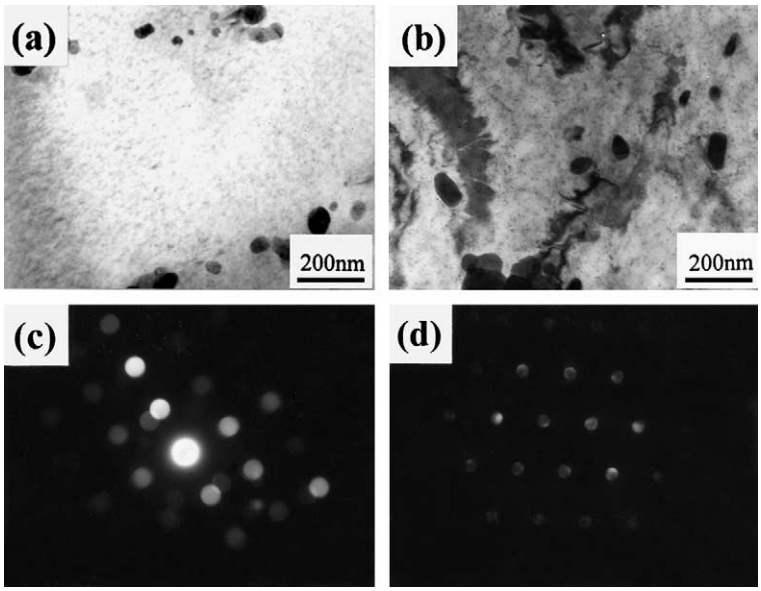

Fig. 13. TEM micrographs of Zr–1Nb–1Sn–0.1Fe–0.5Mo alloy annealed at (a) 600 °C/8h and (b) 600 °C/16 h, and the selected diffraction patterns of the intermetallic compounds: (c) for (a) with a zone axis of $[3\bar{3}02]$ and (d) for (b) with a zone axis of $[1\bar{2}1\bar{3}]$.

perature, transformation of the high-temperature tetragonal ZrO_2 phase to the low-temperature monoclinic ZrO_2 phase may become incomplete if there is a residual compressive stress, thus the tetragonal oxide is retained. Corrosion causes degradation of the oxides such as porosity that diminishes the compressive residual stress, which in turn reduces the volume fraction of the more corrosion-resistant tetragonal oxide. As a consequence, a high corrosion rate ensues.

Finally, the crystallographic texture affects the corrosion properties since the surface energy of crystal planes in Zr is anisotropic and the diffusivity of oxygen ions is also anisotropic. Pemsler et al. [20] reported that the corrosion rate of Zr reached a maximum for the crystal surface for which its c-axis is inclined by 20° to the surface. According to Bibb et al. [14], however, planes like $(0\,0\,0\,1)$ and $(2\,1\,\bar{3}\,0)$ have high resistance to corrosion and $(2\,\bar{3}\,1\,1)$ has the lowest resistance. This is in agreement with the earlier report by Lee and Hwang [13] that asserted $(0\,0\,0\,1)$ plane as the plane of the lowest surface energy. Grain boundary character distribution is another concurrent effect with texture. Depending on the texture, grain boundaries of particular character and energy are exposed to the specimen surface, which affects local diffusion rate of oxygen ions. Mo-addition is known to affect the texture of Zr-base alloy such that f_n of plate-shaped specimen decreases with Mo content [3,21], which was confirmed by the present work (see Fig. 7). With decreasing f_n, the corrosion resistance of Zr-base alloy is expected to deteriorate. It is to be noted that the heat treatment condition of 600 °C/16 h resulted in the best corrosion resistance and also maintained a relatively high f_n value whereas the Mo-containing alloy showed a degraded corrosion resistance due to the low f_n value induced by the partially lath structure remaining from incomplete recrystallization.

An unequivocal solution in optimizing the corrosion resistance of Mo-containing alloys is yet to be found. At present, the particular heat treatment condition quoted above lacks a full explanation on why the desirable microstructural details should be realized. In previous works [22,23], it was reported that the corrosion resistance of ZIRLO alloy sensitively varied with the annealing parameter. This point was checked for the present experimental alloy. In the evaluation of the corrosion resistance of the alloy as a function of the annealing parameter (A), A was defined as

$$A = \sum_i A_i = \sum t_i \exp(-Q/RT_i), \tag{4}$$

where the subscript i refers to the thermal treatment steps involved in the production schedule after β-quenching and the value of Q was taken as 330 kJ/mol. As shown in Fig. 14, there was no clear relationship between the annealing parameter and the corrosion rate.

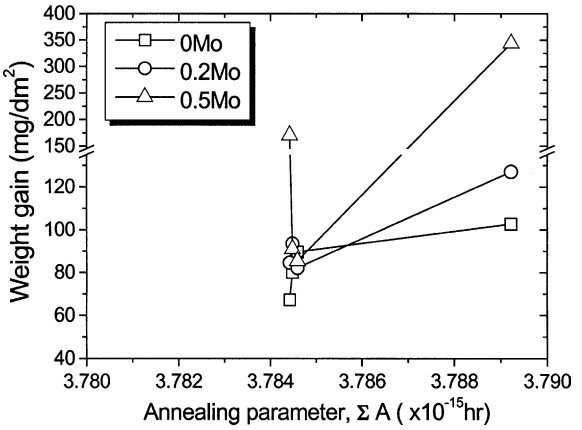

Fig. 14. Effect of the annealing parameter to the corrosion rate of experimental Zr–1Nb–1Sn–0.1Fe–xMo alloys.

It can only be said that extreme value of A is detrimental for corrosion, which is probably due to either insufficient recrystallization (low A) or coarsening of second phase particles and formation of β-Zr (high A).

Overall, the adverse effect of Mo-addition on the corrosion resistance originated from its effect on microstructure and texture. It is necessary, therefore, to circumvent the negative effect by proper treatment, adequate recrystallization at 600 °C/16 h being an example. When this is accomplished, the Zr-base alloys with Mo addition will be attractive for nuclear core applications, considering the high yield strength (thus excessive cold work is unnecessary), microstructural refinement and stability.

5. Conclusions

From the study of the effect of Mo on the microstructure and the corrosion of Zr–1Nb–1Sn–0.1Fe–xMo experimental alloys, the following conclusions were made:

(1) Addition of Mo in Zr–1Nb–1Sn–0.1Fe alloy affects the corrosion resistance when there exists undesirable microstructural features such as heterogeneous distribution of aligned second phase particles, incomplete recrystallization and inadequate texture. These microstructural factors, however, can be alleviated by a proper heat treatment, 600 °C/16 h, for example, so that the corrosion resistance is restored to the level of advanced Mo-free Zr-base alloys.
(2) Morphology and the phase composition, tetragonal vs. monoclinic, of oxides are related to the microstructural characteristics prior to corrosion. Uneven distribution or network structure of β-Zr particles results in lumpy oxides that are associated with the

detrimental corrosion resistance whereas uniform dispersion of second phase particles leads to granular oxides that are associated with the improved corrosion resistance.

(3) Since the corrosion resistance of the Mo-containing experimental alloy can be made at least equal to that of Mo-free Zr–1Nb–1Sn–0.1Fe, the Zr–1Nb–1Sn–0.1Fe–Mo alloy system is worth investigation as a candidate material for nuclear core application, considering other advantages such as the high strength and microstructural stability.

Acknowledgements

This work was performed by the research grant of Korean Institute of Science and Technology Evaluation and Planning under the contract of 1999 Basic Research Program in Atomic Energy Technology and partly through the 2001 National Research Laboratory program.

References

[1] G.P. Sabol, G.R. Kilp, M.G. Balfour, E. Roberts, in: Zirconium in the Nuclear Industry, ASTM STP, vol. 1023, 1989, p. 227.
[2] A.V. Nikulina, V.A. Markelov, M.M. Peregud, Y.K. Bibilashvili, V.A. Kotrekhov, A.F. Lositsky, N.V. Kuzmenko, U.P. Shevnin, V.K. Shamardin, G.P. Kobylyansky, A.F. Lositsky, N.V. Kuzmenko, U.P. Shevnin, V.K. Shamardin, G.P. Kobylyansky, A.E. Novoselov, in: Zirconium in the Nuclear Industry, ASTM STP, vol. 1295, 1996, p. 785.
[3] Y.B. Chun, S.K. Hwang, M.H. Kim, S.I. Kwun, Y.S. Kim, J. Nucl. Mater. 265 (1999) 28.
[4] C.D. Williams, C.E. Ells, P.R. Dixon, Can. Metall. Quart. 11 (1972) 273.
[5] G.J.C. Carpenter, J.F. Watters, in: Zirconium in Nuclear Application, ASTM STP, vol. 551, 1974, p. 400.
[6] Y.B. Chun, S.K. Hwang, M.H. Kim, S.I. Kwun, Scr. Mater. 40 (1999) 1165.
[7] J.H. Lee, S.K. Hwang, K. Yasuda, C. Kinoshita, J. Nucl. Mater. 289 (2001) 334.
[8] G.P. Sabol, R.J. Comstock, R.A. Weiner, P. Larouere, R.N. Stanutz, in: Zirconium in the nuclear industry, ASTM STP, vol. 1245, 1994, p. 724.
[9] S.J. Kim, K.H. Kim, J.H. Baek, B.K. Choi, Y.H. Jeong, Y.H. Jung, J. Nucl. Mater. 256 (1998) 114.
[10] R.J. Comstock, G. Schoenberger, G.P. Sabol, in: Zirconium in the nuclear industry, ASTM STP, vol. 1295, 1996, p. 710.
[11] S. Kass, J. Nucl. Mater. 28 (1969) 315.
[12] Salinas-Rodriguez, Acta Metall. Mater. 43 (1995) 485.
[13] J.I. Lee, K. Kim, S.K. Hwang, Kor. Phys. Soc. 32 (1992) 372.
[14] A.E. Bibb, J.R. Fascia, Trans. Met. Soc. AIME 230 (1964) 415.
[15] R.C. Gravie, P.J. Nickolson, J. Am. Ceram. Soc. 55 (6) (1972) 303.
[16] G. Wikmark, P. Rudling, B. Lehtinen, B. Hutchinson, A. Oscarsson, E. Ahleberg, in: Zirconium in the nuclear industry, ASTM STP, vol. 1295, 1996, p. 55.
[17] V.F. Urbanic, R.W. Gilbert, in: Proceedings of the IEAE Meeting on Fundamental Aspect of Corrosion of Zirconium Base Alloy in Light Water Reactor Environments, 1990, p. 262.
[18] B. Cox, in: M.G. Fontana, R.W. Staehle (Eds.), Advances in Corrosion Science and Technology, vol. V, Plenum, New York, 1976, p. 259.
[19] J. Godlewski, in: Zirconium in the nuclear industry, ASTM STP, vol. 1245, 1994, p. 663.
[20] J.P. Pemsler, J. Electrochem. Soc. 105 (1960) 315.
[21] J.H. Kim, S.K. Hwang, M.H. Kim, S.I. Kwun, Y.S. Kim, J. Kor. Inst. Met. Mater. 35 (1997) 1271.
[22] J.M. Kim, Y.H. Jeong, Y.H. Jung, Met. Mater. 6 (2000) 139.
[23] T. Isobe, T. Matsuo, Y. Mae, in: Zirconium in the nuclear industry, ASTM STP, vol. 1245, 1994, p. 437.